# AN IMPROVED CLUSTER RICHNESS ESTIMATOR

EDUARDO ROZO[1], ELI S. RYKOFF[2], BENJAMIN P. KOESTER[3,4], TIMOTHY MCKAY[5,6,7], JIANGANG HAO[5], AUGUST EVRARD[5,6,7], RISA H. WECHSLER[8], SARAH HANSEN[3,4], ERIN SHELDON[9], DAVID JOHNSTON[10], MATTHEW BECKER[3,4], JAMES ANNIS[11], LINDSEY BLEEM[3], RYAN SCRANTON[12]

*Draft version September 16, 2008*

## ABSTRACT

Minimizing the scatter between cluster mass and accessible observables is an important goal for cluster cosmology. In this work, we introduce a new matched filter richness estimator, and test its performance using the maxBCG cluster catalog. Our new estimator significantly reduces the variance in the $L_X$−richness relation, from $\sigma^2_{\ln L_X} = (0.86 \pm 0.02)^2$ to $\sigma^2_{\ln L_X} = (0.69 \pm 0.02)^2$. Relative to the maxBCG richness estimate, it also removes the strong redshift dependence of the richness scaling relations, and is significantly more robust to photometric and redshift errors. These improvements are largely due to our more sophisticated treatment of galaxy color data. We also demonstrate the scatter in the $L_X$−richness relation depends on the aperture used to estimate cluster richness, and introduce a novel approach for optimizing said aperture which can be easily generalized to other mass tracers.

*Subject headings:* galaxies: clusters – X-rays: galaxies: clusters

## 1. INTRODUCTION

The dependence of the halo mass function on cosmology is a problem that is well understood both analytically (Press & Schechter 1974; Bond et al. 1991; Sheth & Tormen 2002) and numerically (Jenkins et al. 2001; Warren et al. 2006; Tinker et al. 2008). In principle, this detailed understanding allows one to place tight constraints on the amplitude of the primordial power spectrum and on dark energy parameters (e.g. Holder et al. 2001; Haiman et al. 2001). In practice, life is not so simple. Cluster mass is not an observable, and so we must rely on other quantities that trace mass to estimate the halo mass function. In this context, observables that are tightly correlated with mass and whose scatter is well understood are highly desirable, as they permit a more accurate measurement of the mass function.

One such mass tracer, and the subject of interest for this work, is the so called cluster richness, a measure of the galaxy content of a cluster. Relative to other popular mass tracers such as X-ray properties, SZ-decrements, and galaxy velocity dispersion, optical richness has unique advantages and disadvantages. Its unique advantages are:

1. cluster richness can be easily estimated with inexpensive, photometric optical data.

2. cluster richness can be estimated for both massive clusters and low mass groups.

The first of these two properties is significant because it implies that cluster richness estimates are readily available given any large, photometric optical survey such as the SDSS (York et al. 2000a) , DES[13], or LSST[14]. The latter property, on the other hand, is an important advantage for a much more interesting reason.

Beginning with White et al. (1993), cosmological constraints from galaxy clusters have been presented as a degeneracy relation $\sigma_8 \Omega_m^\gamma = constant$ where $\gamma \approx 0.5$, $\sigma_8$ is a parameter specifying the amplitude of the primordial power spectrum, and $\Omega_m$ is the matter density of the universe in units of the critical density. The existence of this degeneracy is easy to explain (Rozo et al. 2004): suppose that we only measured the abundance of galaxy clusters at a single mass scale. Since the halo mass function depends on both $\sigma_8$ and $\Omega_m$, it is evident that with just one observable there must be a degeneracy between these two parameters. But what if we measure the halo mass function over a range of scales? This is roughly equivalent to measuring the amplitude and slope of the halo mass function at the statistical pivot point. If the mass range probed is small, then the slope of the mass function is not well constrained, and the degeneracy between $\sigma_8$ and $\Omega_m$ will remain. In order to break this degeneracy, a measurement of the halo mass function over a large range of masses is necessary. Currently, only spectroscopic velocity measurements and optical richness estimates can probe a mass range wide enough to successfully break this degeneracy, but the former requires considerably more observing resources.

There are, however, important disadvantages to using cluster richness as a mass tracer. For instance, historically, the fact that the relation between cluster richness and mass cannot be predicted a priori based on simple physical arguments was viewed as a significant drawback. Nowadays, however,

[1] Center for Cosmology and Astro-Particle Physics (CCAPP), The Ohio State University, Columbus, OH 43210

[2] TABASGO Fellow, Physics Department, University of California at Santa Barbara, 2233B Broida Hall, Santa Barbara, CA 93106

[3] Department of Astronomy and Astrophysics, The University of Chicago, Chicago, IL 60637

[4] Kavli Institute for Cosmological Physics, The University of Chicago, Chicago, IL 60637

[5] Physics Department, University of Michigan, Ann Arbor, MI 48109

[6] Astronomy Department, University of Michigan, Ann Arbor, MI 48109

[7] Michigan Center for Theoretical Physics, Ann Arbor, MI 48109

[8] Kavli Institute for Particle Astrophysics & Cosmology, Physics Department, and Stanford Linear Accelerator Center, Stanford University, Stanford, CA 94305

[9] Center for Cosmology and Particle Physics, Physics Department, New York University, New York, NY 10003

[10] Jet Propulsion Laboratory, 4800 Oak Grove Drive, Pasadena, CA 91109

[11] Fermi National Accelerator Laboratory, P.O. Box 500, Batavia, IL 60510

[12] Department of Physics and Astronomy, Universityof Pittsburgh, 3941 O'Hara St., Pittsburgh, PA 15260

[13] http://www.darkenergysurvey.org/
[14] http://www.lsst.org/lsst_home.shtml

this argument holds little sway, since the level of accuracy required for precision comsology in our a priori knowledge of cluster scaling relations is pushing current research towards a self-calibrating approach, in which both cosmology and cluster scaling relations are simultaneously constrained from the data (Lima & Hu 2004; Majumdar & Mohr 2004; Lima & Hu 2005; Hu & Cohn 2006; Wu et al. 2008). Thus, in so far as self-calibration is necessary to insure one-self against possible biases in cosmological estimates, the lack of a simple physical model for predicting cluster richness is no longer a serious drawback.

Another reason why optical richness estimates fell out of favor relative to other mass tracers is that, in the past, richness estimates were known to suffer from significant projection effects, which resulted in impure cluster samples as well as large scatter in the mass-richness relation. Abell made one of the first systematic attempts at measuring richness (Abell 1958; Abell et al. 1989) in defining his richness classes. He tried to minimize projection by only counting galaxies dimmer than $m_3$, the magnitude of the third brightest cluster galaxy, but brighter than $m_3 + 2$. The bright cut is aimed at foreground interlopers, while the dim cut reduces the contribution of the galaxy background. Later methods used similar counting techniques but included a proper account of the background (e.g. Bahcall 1981) . Since then, more sophisticated algorithms have been developed and applied to CCD-based imaging (e.g. matched-filter methods Postman et al. 1996; Bramel et al. 2000; Yee & López-Cruz 1999; Kochanek et al. 2003; Dong et al. 2008).

Projection effects are now a much more benign problem thanks to these more sophisticated richness measurement techniques, the advent of accurate photometric data enabled by modern CCDs, and most recently, the well-known observations that ellipticals and cluster E/S0 galaxies in particular tend to form a tight ridgeline in color-magnitude space (Visvanathan & Sandage 1977; Bower et al. 1992; Gladders & Yee 2000; Koester et al. 2007b). This color clustering has been integral to richness measurements in the SDSS (Goto et al. 2002; Miller et al. 2005; Koester et al. 2007b) and the Red Sequence Cluster Survey (RCS: Gladders & Yee 2005), and such color-based measures have been shown to be effective mass tracers (Yee & Ellingson 2003; Muzzin et al. 2007; Sheldon et al. 2007a; Johnston et al. 2007; Rykoff et al. 2008b; Becker et al. 2007a).

While richness estimates show a strong correlation with other mass proxies (e.g. Yee & Ellingson 2003; Dai et al. 2007; Sheldon et al. 2007a; Johnston et al. 2007; Becker et al. 2007a; Rykoff et al. 2008a), considerable scatter in the mass–richness relation still remains. For instance, the richness measure used in the RCS cluster catalog has a logarithmic scatter of $\sigma_{\ln M} \approx 0.8$ (Gladders et al. 2007), while for maxBCG clusters the number is closer to $\sigma_{\ln M} \approx 0.5$ (Rozo et al. 2008). This is to be compared to the scatter for X-ray mass tracers, which is expected to be as low as $\approx 8\%$ for $Y_X$ based on simulations (Kravtsov et al. 2006), or as high as $\approx 25\%$ for non-core extracted soft X-ray band luminosities (e.g. Stanek et al. 2006; Vikhlinin et al. 2008a). Clearly, much improvement is needed to bring the scatter of richness measures to the level of X-ray mass tracers.

This work is aimed at reducing the variance in the richness-mass relation. We do this by explicitly constructing a new richness estimator that significantly reduces the scatter in mass at fixed richness for maxBCG clusters. Relative to $N_{200}$ of maxBCG, we introduce two significant differences. The

first of these involves using a matched filter algorithm to estimate cluster richness. Matched filters have been used in the literature before (Postman et al. 1996; Kochanek et al. 2003). Unlike those works, however, our matched filter includes a color component, which is of critical importance for reducing projection effects over the redshift range spanned by our cluster sample.[15] In that sense, our filter is closer in spirit to that of Dong et al. (2008), who include a photometric redshift filter into their richness estimate. We also note here that group-scale studies suggest that some measure of the average color in the cluster is indicative of mass, particularly below $\sim 10^{14} M_\odot$ (Martínez et al. 2002; Martínez & Muriel 2006; Weinmann et al. 2006; Hansen et al. 2007) .

The second difference we introduce is the way in which the aperture used to estimate cluster richness is determined. Generically, cluster richness estimators involve counting the number of galaxies within some specified aperture, which can thus be interpreted as defining the "size" of the cluster. This begs the question, then, of how is one to select the correct size of a cluster a priori? Theoretically, halo sizes are usually defined in terms of $R_\Delta$, a radius which encompasses a mean density that is $\Delta$ times either the mean or the critical density of the universe (conventions vary from author to author). Unfortunately, not only is such a definition not applicable observationally, authors vary both on the reference background density (critical versus mean mass density), and on the specific overdensity value. Thus, even though significant progress has been made (Cuesta et al. 2008), a definitive definition of halo size remains elusive.

In this work, we approach this question with observations in mind. That is, rather than coming with a preconceived notion of what the radius of a cluster is, we let the data tell us what the optimal radii for our clusters is by demanding that optical richness be as tightly correlated as possible with X-ray luminosity. The idea is as follows: first, one posits a scaling relation between cluster richness and cluster radius. When estimating cluster richness, one then demands that the richness-radius scaling relation be satisfied. For instance, given a cluster, one can simply make an initial guess for its richness. Using the richness-radius scaling relation, one can then draw a circle of the appropriate radius, and count the number of galaxies within it. If the richness was underestimated, one will find too many galaxies, signaling that the richness estimate must be increased. Proceeding in this way, one can quickly zero in on the appropriate richness for the object.

This does, however, leave open the question of what the correct richness-radius relation is. Since we are interested in finding a new richness estimator that is tightly correlated with halo mass, we can use the scatter in the mass–richness relation as our figure of merit to determine the "correct" richness-radius relation. In practice, we use the $L_X$−richness scatter rather than the mass–richness scatter because the scatter in mass is not directly observable. We emphasize that since the mass scatter at fixed X-ray luminosity (see e.g. Vikhlinin et al. 2008b) is considerably tighter than the corresponding scatter at fixed richness (Rozo et al. 2008), the use of X-ray luminosity as a mass tracer for our purposes is well justified.

The layout of the paper is as follows. We describe the data sets used in this work in § 2. Our matched filter estimator is introduced in § 3, followed by our method for determining the

---

[15] In Kochanek et al. (2003), the low redshift of the clusters make single band magnitudes better proxies for distance than colors, so the lack of a color filter in the richness estimator is less important for their work.

optimal radius-richness relation in § 4. We present our results in section § 5. In investigating the properties of our new richness measure, we have discovered that the redshift evolution of the richness-mass relation of our new estimator is much more mild than that measured for $N_{200}$. These results and the corresponding discussion are presented in § 6. We summarize our results and present our conclusions in § 7. Throughout, whenever needed a flat $\Lambda$CDM cosmology with $\Omega_M = 0.3$ and $h = 1.0$ was assumed.

## 2. DATA

The data for the analysis presented in this work comes from two large area surveys, the Sloan Digital Sky Survey (SDSS: York et al. 2000b) and the ROSAT All-Sky Survey (RASS: Voges et al. 1999). SDSS imaging data are used to select clusters and to measure their matched filter richness; RASS data provide 0.1-2.4 keV X-ray fluxes, which we convert into estimates of the X-ray luminosity of the clusters.

### 2.1. SDSS

The imaging and spectroscopic surveys that comprise the SDSS are currently in the sixth Data Release (Adelman-McCarthy et al. 2008). This release includes nearly 8500 square degrees of drift-scan imaging in the the Northern Galactic Cap, and another 7500 square degrees of spectroscopic observations of stars, galaxies, and quasars.

The camera design (Gunn et al. 2006) and drift-scan imaging strategy of the SDSS enable acquisition of nearly simultaneous observations in the $u, g, r, i, z$ filter system (Fukugita et al. 1996). Calibration (Hogg et al. 2001; Smith et al. 2002; Tucker et al. 2006), astrometric (Pier et al. 2003), and photometric (Lupton et al. 2001) pipelines reduce the data into object catalogs containing a host of measured parameters for each object.

The maxBCG cluster sample and the galaxy catalogs used to remeasure cluster richness in this paper are derived from the SDSS. The galaxy catalogs are drawn from an area approximately coincident with DR4 (Adelman-McCarthy et al. 2006). Galaxies are selected from SDSS object catalogs as described in (Sheldon et al. 2007b). In this work we use `CMODEL_COUNTS` as our total magnitudes, and `MODEL_COUNTS` when computing colors. Bright stars, survey edges and regions of poor seeing are masked as previously described (Koester et al. 2007a; Sheldon et al. 2007b).

### 2.2. Cluster Sample

We obtain sky locations, redshift estimates, and initial richness values from the maxBCG cluster catalog. Details of the selection algorithm and catalog properties are published elsewhere (Koester et al. 2007a,b). In brief, maxBCG selection relies on the observation that the galaxy population of rich clusters is dominated by luminous, red galaxies clustered tightly in color (the E/S0 ridgeline). Since these galaxies have old, passively evolving stellar populations, their $g - r$ color closely reflects their redshift. The brightest such red galaxy, typically located at the peak of the galaxy density, defines the cluster center.

The maxBCG catalog is approximately volume limited in the redshift range $0.1 \le z \le 0.3$, with very accurate photometric redshifts ($\delta z \sim 0.01$). Studies of the maxBCG algorithm applied to mock SDSS catalogs indicate that the completeness and purity are very high, above 90% (Koester et al. 2007a; Rozo et al. 2007). The maxBCG catalog has been used to investigate the scaling of galaxy velocity dispersion

with cluster richness (Becker et al. 2007b) and to derive constraints on the power spectrum normalization, $\sigma_8$, from cluster number counts (Rozo et al. 2007).

The primary richness estimator used in the maxBCG catalog is $N_{200}$, defined as the number of galaxies with $g - r$ colors within $2\sigma$ of the E/S0 ridgeline as defined by the BCG color, brighter than $0.4L_*$ (in $i$-band), and found within $r_{200}^{gal}$ of the cluster center. $r_{200}^{gal}$ is a cluster radius that depends upon the number of galaxies within a fixed aperture 1 $h^{-1}$ Mpc of the BCG, labeled $N_{gals}$, with the relation $r_{200}^{gal}(N_{gals})$ being calibrated so that, on average, the galaxy overdensity within $r_{200}^{gal}$ is $200\Omega_m^{-1}$ assuming $\Omega_m = 0.3$ (Hansen et al. 2005). The full catalog comprises $13,823$ objects with a richness threshold $N_{200} \ge 10$, corresponding to $M \gtrsim 5 \cdot 10^{13} \ h^{-1} \ M_\odot$ (Johnston et al. 2007).

As mentioned in the introduction, we re-estimate the cluster richness for every object in the maxBCG catalog, and measure the corresponding scatter in the $L_X$−richness relation. When doing so, we always limit ourself to the 2000 richest clusters, ranked according to the new richness estimate. This cut is made to ensure that our results are insensitive to the $N_{200} \ge 10$ cut of the maxBCG catalog. That is, the number of clusters with $N_{200} \ge 10$ that fall within the 2000 richest clusters for any of the new richness measures considered has no impact on the recovered scatter. We also note that our choice of always selecting the 2000 richest clusters also implies that the specific cluster sample used to estimate the scatter in the $L_X$−richness relation varies somewhat as we vary the richness estimator.

### 2.3. X-ray Measurements

The scatter in $L_X$ at fixed richness is estimated using a slight variant of the method presented in Rykoff et al. (2008b). Briefly, we use the RASS photon maps to estimate the 0.5-2.0 keV X-ray flux at the location of each cluster, which is used to derive $L_X$ [0.1-2.4 keV] using the cluster photometric redshift (the conversion factors are similar to those used in Böhringer et al. 2004). We then perform a Bayesian linear least squares fit to $\ln L_x$ as a function of $\ln N$, where $N$ is the richness parameter to be tested. The variance in $\ln L_X$ is included as a free parameter. The fit is done following the algorithm presented in Kelly (2007), and correctly takes into account upper limits for $L_X$ for those clusters with upper limits on X-ray emission.

It is important to note here that the estimated X-ray luminosity of a cluster depends on the aperture used to measure $L_X$. Rykoff et al. (2008b) used a fixed 750 $h^{-1}$ kpc aperture as a compromise between needing a large aperture to avoid losing X-ray photons due to the ROSAT PSF and cluster miscentering, and the need for a small aperture in order to increase the signal to noise of the cluster emission. Further work has shown that the scatter in $L_X$ at fixed $N_{200}$ is minimized when using an aperture of 1 $h^{-1}$ Mpc. The corresponding scatter for the top 2000 maxBCG clusters is $\sigma_{\ln L_X | N_{200}} = 0.96 \pm 0.03$.[16]

The nature of the present exercise has the benefit of assigning a cluster radius $R_c$, to each individual cluster, so it is natural to measure $L_X$ in the same scale as the optical rich-

---

[16] The attentive reader will note that the quoted scatter in $L_X$ at fixed richness is significantly larger than the scatter in mass at fixed richness quoted in the introduction, which was closer to 0.5. Given a slope of $\approx 1.6$ in the $L_X - M$ relation, a scatter of 0.96 in $L_X$ corresponds to $\approx 0.96/1.6 \approx 0.6$ scatter in mass. The remaining 10% difference is because the scatter in Rozo et al. (2008) uses the scatter of the 1000 richest clusters, which is smaller than that of the 2000 richest clusters by 0.1.

ness. Thus, in this work, we estimate $L_X$ using a variable aperture which depends upon the cluster's richness. Using a fixed $1\,h^{-1}$ Mpc aperture to estimate $L_X$ does not have a large effect on our results, for reasons that will be discussed below. Finally, we note that very small physical apertures are impractical for the most distant clusters due to the large size of the RASS PSF, which corresponds to a physical scale of $300\,h^{-1}$ kpc (FWHM) at $z = 0.23$, the median redshift of the maxBCG catalog. Therefore, we place a fixed minimum aperture of $500\,h^{-1}$ kpc for each cluster. We discuss the small effect of this aperture cutoff in § 4.

### 2.4. *Cleaning the Sample*

Our analysis depends on a combination of optical and X-ray measurements of maxBCG clusters using SDSS and RASS data. As discussed in detail in Rykoff et al. (2008b, see § 5.6), there is clear evidence that cool core clusters increase the scatter in X-ray cluster properties. High resolution X-ray imaging of clusters allows the exclusion of cluster cores, reducing the scatter in observed X-ray properties (e.g. O'Hara et al. 2006; Chen et al. 2007; Maughan 2007). Unfortunately, the broad PSF of RASS means that it is impossible to exclude the cores of clusters in this work. In order to asses how robust our results are to the presence or absence of cooling flow clusters in the cluster sample, we have created a "clean" sample of maxBCG clusters by removing all known cool core clusters that might have boosted global X-ray luminosity and may significantly bias our results. In addition, we have removed apparently X-ray bright maxBCG clusters that were determined via inspection to have their X-ray flux significantly contaminated by foreground objects such as stars, low redshift galaxy clusters, and AGN.

There does not exist a complete, unbiased catalog of cool core X-ray clusters. The presently described cleaning procedure is not intended to be complete, and is intended only to give some sense of the robustness of our results to the presence of cooling flow clusters. Following Rykoff et al. (2008b), we have assembled all the known cool core clusters from the literature. This includes: A750, A1835, Z2701, Z3146, Z7160, RXC 2129.6+0005 (Bauer et al. 2005), A1413 (Chen et al. 2007), A2244 (Peres et al. 1998), and RXC J1504.1−0248 (Böhringer et al. 2005). From here on, the maxBCG catalog presented in Koester et al. (2007b) is referred to as the "full" cluster sample, and the subsample described above is referred to as the "clean" cluster sample.

### 3. MATCHED FILTER RICHNESS ESTIMATORS

### 3.1. *Derivation of the Matched Filter Richness Estimator*

Let $\mathbf{x}$ be a vector characterizing the observable properties of a galaxy (e.g. galaxy color and magnitude). We model the projected galaxy distribution around clusters as a sum $S(\mathbf{x}) = \lambda u(\mathbf{x}|\lambda) + b(\mathbf{x})$ where $\lambda$ is the number of cluster galaxies, $u(\mathbf{x}|\lambda)$ is the cluster's galaxy density profile normalized to unity, and $b(\mathbf{x})$ is density of background (i.e. non-member) galaxies. The probability that a galaxy found near a cluster is actually a cluster member is given by

$$p(\mathbf{x}) = \frac{\lambda u(\mathbf{x}|\lambda)}{\lambda u(\mathbf{x}|\lambda) + b(\mathbf{x})}. \qquad (1)$$

Consequently, the total number of cluster galaxies $\lambda$ must satisfy the constraint equation

$$\lambda = \sum p(\mathbf{x}|\lambda) = \sum \frac{\lambda u(\mathbf{x}|\lambda)}{\lambda u(\mathbf{x}|\lambda) + b(\mathbf{x})} \qquad (2)$$

where the sum is over all galaxies in the cluster field. If the filters $u(\mathbf{x}|\lambda)$ and $b(\mathbf{x})$ are known, then given an observed galaxy distribution $\{\mathbf{x}_1, ..., \mathbf{x}_N\}$ around a cluster we can define a richness estimator $\hat{\lambda}$ as the solution to equation 2. As it turns out, one can also derive this expression using a maximum likelihood approach. Interested readers are referred to appendix A for details. From now on, the letter $\lambda$ shall always refer to a matched filter richness estimate obtained with equation 2.

### 3.2. *Cluster Radii and Matched Filter Richness Estimates*

Consider again Eqn. 2. As mentioned before, the sum used in Eqn. 2 needs to extend over all galaxies. In practice, of course, one needs to add over all galaxies within some cutoff radius $R_c$. Operationally, this is equivalent to setting $u = 0$ for all galaxies with radii $R > R_c$, so it is natural to interpret the cutoff radius $R_c$ as a cluster radius. In this light, it seems obvious that considerable care must be taken to choose the correct cluster radius when estimating richness, but how to go about doing just that is a less straightforward question.

In this work, we propose that cluster radii be selected on the basis of a model radius-richness relation. Specifically, we assume that the size of a cluster of richness $\lambda$ scales as a power law of $\lambda$,

$$R_c(\lambda) = R_0(\lambda/100.0)^{\alpha}. \qquad (3)$$

Naively, we expect $R_0 \approx 1$ Mpc, as that is the characteristic size of clusters, and $\alpha \approx 1/3$ assuming that $R \propto M^{1/3} \propto \lambda^{1/3}$. We postpone the discussion of how we go about selecting $R_0$ and $\alpha$ to section 4. For the time being, we shall simply assume that $R_0$ and $\alpha$ are known. In that case, equation 2 becomes

$$\lambda = \sum p(\mathbf{x}|\lambda) = \sum_{R < R_c(\lambda)} \frac{\lambda u(\mathbf{x}|\lambda)}{\lambda u(\mathbf{x}|\lambda) + b(\mathbf{x})}. \qquad (4)$$

Note that we have explicitly included the cutoff radius $R_c$ in the sum above, and that this cutoff radius now depends on $\lambda$. Moreover, one can see that in the above equation, *the cluster richness $\lambda$ is the only unknown*, so we can numerically solve for $\lambda$. In other words, by positing a richness-radius relation we are able to simultaneously estimate both a cluster radius and the corresponding cluster richness.[17]

### 3.3. *The Filters*

In this work we consider three observable properties of galaxies: $R$, the projected distance from a galaxy to the assigned cluster center, $m$, the galaxy magnitude, and $c$, the galaxies' $g - r$ color. We adopt a separable filter function

$$u(\mathbf{x}) = [2\pi R\Sigma(R)]\phi(m)G(c) \qquad (5)$$

where $\Sigma(R)$ is the two dimensional cluster galaxy density profile, $\phi(m)$ is the cluster luminosity function (expressed in apparent magnitudes), and $G(c)$ is color distribution of cluster galaxies. The prefactor $2\pi R$ in front of $\Sigma(R)$ accounts for the fact that given $\Sigma(R)$, the radial probability density distribution is given by $2\pi R\Sigma(R)$. Also, note the separability condition makes the implicit assumption that these three quantities are fully independent of each other, which is not true in detail (for a discussion of the galaxy population of maxBCG clusters see Hansen et al. 2007). For instance, the tilt of the ridgeline

---

[17] Note that since we are explicitly setting $u = 0$ for $R > R_c$, the fact that $u$ must be normalized to unity necessarily introduces a dependence of $u$ on $\lambda$. That is, changing $\lambda$ will not only change the range of the sum in equation 4, it will also change the value of the summands.

implies that the mean color of a red sequence cluster galaxy varies slightly as a function of magnitude. We postpone an investigation of how including the correlation between these various observables affects our conclusions to future work (Koester et al, in preparation). We now describe each of our three filters in detail. We note that defining said filters requires us to specify parameters governing the shape of the filters (e.g. $R_s$ for the radial filter, $\alpha$ for the luminosity filter, etc.). A detailed study on the dependence of our matched filter richness estimates on the shape of our filters will be presented in future work.

### 3.3.1. *The Radial Filter*

N-body simulations show that the matter distribution of massive halos can be well described by the so called NFW profile (see e.g. Navarro et al. 1995, 1997),

$$\rho(r) \propto \frac{1}{(r/r_s)(1+r/r_s)^2} \quad (6)$$

where $r_s$ is characteristic scale radius at which the logarithmic slope of the density profile is equal to $-2$. The corresponding two dimensional surface density profile (Bartelmann 1996) is

$$\Sigma(R) \propto \frac{1}{(R/R_s)^2-1} f(R/R_s) \quad (7)$$

where $R_s = r_s$ and

$$f(x) = 1 - \frac{2}{\sqrt{x^2-1}} \tan^{-1}\sqrt{\frac{x-1}{x+1}}. \quad (8)$$

This formula assumes $x > 1$. For $x < 1$, one uses the identity $\tan^{-1}(ix) = i\tanh(x)$.

Here, we assume that the NFW profile can also reasonably describe the density distribution of galaxies in clusters (Lin & Mohr 2004; Hansen et al. 2005; Popesso et al. 2007), and follow Koester et al. (2007a) in setting $R_s = 150\ h^{-1}$ kpc. In principle, one could optimize the value of this parameter, but we do not expect our final results to be overly sensitive to our chosen value (see e.g. Dong et al. 2008). Also, in order to avoid the singularity at $R = 0$ in the above expression, we set $\Sigma$ to a constant for $R \leq R_{core} = 100\ h^{-1}$ kpc. This core density is chosen so that the mass distribution $\Sigma(R)$ is continuous. Our results are insensitive to the particular choice of core radius for $R_{core} \leq 200\ h^{-1}$ kpc. Finally, the profile $\Sigma(R)$ is truncated at the cluster radius $R_c(\lambda)$, and is normalized such that

$$1 = \int_0^{R_c(\lambda)} dR\, 2\pi R\Sigma(R). \quad (9)$$

We emphasize that this condition implies that the normalization constant for the density profile is richness dependent, and must be recomputed for each $\lambda$ value when solving for $\lambda$ in equation 4.

### 3.3.2. *The Luminosity Filter*

At $z \lesssim 0.3$, the luminosity distribution of satellite cluster galaxies is well-represented by a Schechter function (e.g Hansen et al. 2007) which we write as

$$\phi(m) = 0.4\ln(10)\phi_* 10^{-0.4(m-m_*)(\alpha+1)} \exp\left(-10^{-0.4(m-m_*)}\right) \quad (10)$$

We take $\alpha = 0.8$ independent of redshift. The characteristic magnitude, $m_*$, is corrected for the distance modulus, k-corrected, and passively-evolved using stellar population synthesis models described in Koester et al. (2007b). When applying the luminosity filter, $m_*$ is chosen from these models,

appropriate to the redshift of the cluster under consideration, and the filter is normalized by integrating down to a magnitude corresponding to $0.4L_*$ at the cluster redshift, or an absolute magnitude $M_i = -20.25$. The latter is simply a luminosity cut bright enough to make the maxBCG sample volume limited.

### 3.3.3. *The Color Filter*

Early type galaxies are known to dominate the inner regions of low redshift galaxy clusters (see e.g. Dressler 1984; Kormendy & Djorgovski 1989; Hansen et al. 2007). The rest-frame spectra of these galaxies typically exhibit a significant drop at about 4000 Å, that gives early type galaxies at the same redshift nearly uniformly red colors when observed through filters that encompass this break. In the SDSS survey, the corresponding filters for galaxies at $z \lesssim 0.35$ are $g$ and $r$, and we find that the $g-r$ colors of early type galaxies are found to be gaussianly distributed with a small intrinsic dispersion of about 0.05 magnitudes. Consequently, we take the color filter $G(c)$ to be

$$G(c|z) = \frac{1}{\sqrt{2\pi}\sigma} \exp\left[\frac{(c-\langle c|z\rangle)^2}{2\sigma^2}\right] \quad (11)$$

where $c = g-r$ is the color of interest, $\langle c|z\rangle$ is the mean of the Gaussian color distribution of early type galaxies at redshift $z$, and $\sigma$ is the width of the distribution. The mean color $\langle c|z\rangle = 0.625 + 3.149z$ was determined by matching maxBCG cluster members to the SDSS LRG (Eisenstein et al. 2001) and MAIN (Strauss et al. 2002) spectroscopic galaxy samples. The net dispersion $\sigma$ is taken to be the sum in quadrature of the intrinsic color dispersion $\sigma_{int}$, set to $\sigma_{int} = 0.05$, and the estimated photometric error $\sigma_m$. In $g-r$, the typical photometric error on the red-sequence cluster galaxies brighter than $0.4L_*$ is $\sigma_m \approx 0.01$ magnitudes for $z = 0.1$, but can be as as large as $\sigma_m \approx 0.05$ magnitudes for $z = 0.3$.

### 3.3.4. *Background Estimation*

To fully specify our filters, we also need to describe our background model. We assume the background galaxy density is constant in space, so that $b(\mathbf{x}) = 2\pi R\bar{\Sigma}_g(m_i, c)$ where $\bar{\Sigma}_g(m_i, c)$ is the galaxy density as a function of galaxy $i$–band magnitude and $g-r$ color. $\bar{\Sigma}_g(m_i, c)$ is estimated by distributing $10^6$ random points throughout the same SDSS photometric survey footprint that defines our galaxy sample. All galaxies within an angular separation of 0.05 degrees of the random points (about $1h^{-1}$ Mpc at $z = 0.25$) are used to empirically determine the mean galaxy density $\bar{\Sigma}_g(m_i, c)$ using a top hat cloud-in-cells (CIC) algorithm (e.g. Hockney & Eastwood 1981). For our cells, we used 60 evenly-spaced bins in $g-r \in [0, 2]$ and 40 bins in $i \in [14, 20]$. In each 2 dimensional bin, the number density of galaxies is normalized by the total number of random points, the width of each color and magnitude bin (0.05 mags and 0.1 mags, respectively), and area searched ($0.05^2\pi$ degrees).

This process creates an estimate of the global background, i.e. the number density of galaxies as a function of color and magnitude in the full SDSS survey. Not surprisingly, a similar result is obtained by binning the whole galaxy catalog in color and magnitude with CIC and dividing by the survey area. However, the procedure we employ above can readily be adapted to returning alternative background estimates, e.g the local cluster density as a function of redshift, by replacing random points with clusters.

### 4. METHODS

We have now fully specified our richness estimators, except for the values $R_0$ and $\alpha$ that govern the radius-richness scaling relation. We now discuss how we go about selecting optimal values for these parameters.

As we mentioned earlier, we wish to find the cluster richness estimator that minimizes the scatter in the richness-mass relation. Cluster mass, however, is not an observable, and thus we must rely on other mass tracers. Here, we use X-ray luminosity ($L_X$) as our mass proxy, primarily because it is a well known mass tracer (e.g. Reiprich & Böhringer 2002; Stanek et al. 2006; Rykoff et al. 2008a) that is readily accessible to us and for which we can quickly estimate the scatter for multiple richness measures (see Rykoff et al. 2008b).

We proceed as follows: we begin by defining a coarse grid in $R_0$ and $\alpha$, given by

$$R_0 = \{0.5, 0.75, 1.0, 1.25, 1.5\} \tag{12}$$
$$\alpha = \{-0.05, 0.05, 0.15, 0.25, 0.35, 0.45\} \tag{13}$$

where $R_0$ is measured in units of $h^{-1}$ Mpc. Each of these grid points defines a distinct richness estimator through equation 4. For each grid point, we estimate the corresponding richness for every cluster in the maxBCG catalog. We then select the 2000 richest clusters and calculate the scatter in $L_X$ at fixed richness of those top 2000 clusters. Note that, because the rank ordering of the clusters changes as we vary our richness estimate, the clusters used to estimate the scatter in $L_X$ varies slightly across the grid. We limit ourselves to the richest 2000 clusters to ensure our results are insensitive to the $N_{200} \geq 10$ cut in the maxBCG catalog.

From our measurements of the scatter $\sigma_{\ln L_X|\lambda}(R_0, \alpha)$ at each grid point, we can directly read which parameter combination minimizes the scatter. We emphasize that because the scatter in mass at fixed $L_X$ is much lower than the corresponding scatter at fixed richness (Rozo et al. 2008), for our purposes $L_X$ is a nearly perfect mass tracer. We note that the X-ray measurements described in 2.3 require a minimum aperture of $500\,h^{-1}$ kpc. For the 2000 richest clusters, this cutoff is only employed when $R_0 = 0.5\,h^{-1}$ Mpc and $\alpha \geq 0.15$, which is a region of parameter space that already does not appear to have a strong correlation between $L_X$ and richness. Therefore, we conclude that the aperture cutoff does not have a significant effect on our results.

To determine the uncertainty in the recovered parameters $R_0$ and $\alpha$, we need to understand the errors in our measurement of the Lx-richness scatter. We estimate these errors using bootstrap resampling. We proceed as follows: let $\mu$ be an index that runs over all grid points $(R_0, \alpha)$, and $\sigma_\mu$ be the scatter at the $\mu^{th}$ grid point. We resample (with replacement) the full maxBCG catalog, and measure the scatter $\sigma_\mu$ at every grid point. The procedure is iterated 100 times, and the measurements are used to estimate the mean and covariance matrix of $\sigma_\mu$.[18] Assuming that the probability distribution $P(\sigma_\mu)$ is a multi-variate Gaussian characterized by the observed mean and covariance matrix, we generate $10^5$ Monte Carlo realizations of the scatter, and estimate the fraction of times that each grid point is observed to have the lowest scatter among all grid points.

To use the grid to zero in on a particular value for $R_0$ and $\alpha$, and to estimate errors in these values, we fit each of the $10^5$

---

[18] The measurement of the scatter in $L_X$ at fixed richness is very time consuming, and needs to be done independently for every point in the grid. This explains why we restrict ourselves to only 100 bootstrap resamplings.

---

realizations of the scatter $\sigma_{\ln L_X|\lambda}(R_0, \alpha)$ with a 2D parabola. From the fits, we can read off the values of $R_0$ and $\alpha$ at which the minimum occurs, giving us $10^5$ samplings of the probability distribution of the location of the minimum in parameter space. The probability distribution of the resulting $10^5$ minima is exactly what we desired.

As it turns out, and as discussed in § 5, the coarse grid defined above is too broad for a parabolic fit to adequately describe the function $\sigma_{\ln L_X|\lambda}(R_0, \alpha)$. However, if we restrict ourselves to a smaller region of parameter space near the minimum determined from the coarse grid, a quadratic fit becomes adequate. Therefore, we have defined a narrower fine grid,

$$R_0 = \{1.0, 1.1, 1.2, 1.3, 1.4\} \tag{14}$$
$$\alpha = \{0.22, 0.26, 0.30, 0.34, 0.38, 0.42\} \tag{15}$$

with $R_0$ measured in units of $h^{-1}$ Mpc. It is this grid that we use to report our final results and to select the optimal parameters $R_0$ and $\alpha$.

To summarize, we first do a rough exploration of the parameter space $R_0$ and $\alpha$ using a coarse grid, and then use a smaller but finer grid to statistically constrain the location of the scatter minimum.

### 5. RESULTS

#### 5.1. The Full Sample

Figure 1 illustrates the probability that each coarse grid point is found to minimize the scatter of the 2000 richest clusters when resampling our data as described in § 4. For this plot, we have used the full cluster sample, though a similar result holds when using the clean cluster sample. Each square is shaded in gray on a log scale according to the fraction of trials that point is found to have the minimum scatter. The primary feature of this plot is a broad degeneracy region from $(R_0, \alpha) \approx (0.8, 0.0)$ to $(R_0, \alpha) \approx (1.4, 0.5)$, corresponding to a scatter $\sigma_{\ln L_X|\lambda} \approx 0.78$. Note this scatter is a significant improvement relative to the $L_X$−richness scatter measured for $N_{200}$, $\sigma_{\ln L_X|N_{200}} = 0.96$. The scatter in $L_X$ increases as we move away from the degeneracy region, ranging from $\sigma_{\ln L_X|\lambda} \sim 0.86$ in the lower-right corner of Figure 1 to $\sigma_{\ln L_X|\lambda} > 1.0$ in the upper-left corner. Further discussion of why our new richness estimator results in significantly reduced scatter is presented in § 6.

Figure 2 shows the probability density of the points in $R_0 - \alpha$ space that minimize the scatter in $L_X$ at fixed richness for the fine grid, as estimated through the parabolic fits to the function $\sigma_{\ln L_X|\lambda}(R_0, \alpha)$ described in section § 4. The solid contours are for the full cluster sample and the dashed contours are for the clean cluster sample. The diagonal degeneracy suggested in the previous plot is now very obvious, especially in the $2\sigma$ contour. Importantly, both the full and clean sample produce very similar results, although the contours are noticeably smoother for the clean sample. We note that the closing of the $1\sigma$ contours in the upper-right and lower-left is likely an artifact of the grid boundaries. As demonstrated in the coarse grid in Figure 1, the degeneracy region extends at least to $\alpha \sim 0$ and $\alpha \sim 0.5$.

The existence of the degeneracy region is relatively simple to explain. Consider the problem we are trying to address: what is the correct size of a cluster? Roughly speaking, this involves two parts: one, determining the correct cluster size of the average cluster, and two, determining how the cluster size scales with richness as one moves away from the average cluster. The former is much better determined than the lat-
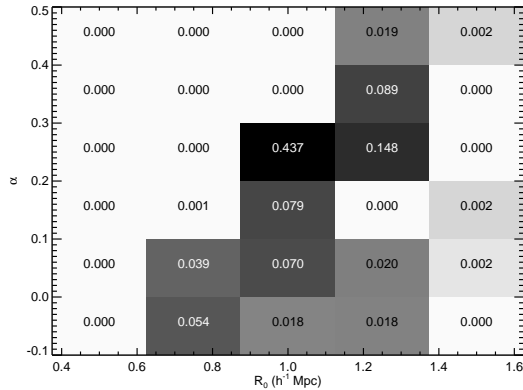
FIG. 1.— Probability that a given point in the grid minimizes the scatter in $L_X$ at fixed richness in the coarse grid. The gray scale varies logarithmically with the probability, which is explicitly quoted in the Figure. Note the broad degeneracy region from $(R_0, \alpha) \approx (0.8, 0.0)$ to $(R_0, \alpha) \approx (1.4, 0.5)$, where the scatter $\sigma_{\ln L_X | \lambda} \sim 0.78$.
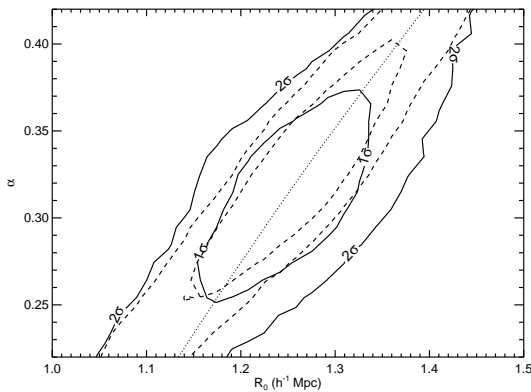


FIG. 2.— Contour plot of the probability density of the points in $R_0 - \alpha$ space that minimize the scatter $\sigma_{\ln L_X | \lambda}(R_0, \alpha)$. The solid contours show the $1\sigma$ and $2\sigma$ contours for the full sample, and the dashed lines show the same contours for the "cleaned" sample (see § 2.4). The closing of the $1\sigma$ contours in the upper-right and lower-left are likely an artifact of the grid. The dotted line shows the contour of fixed mean cluster radius $R_c = 900 \, h^{-1}$ kpc. All the richness estimators along this line result in the same mean cluster radius, and have therefore very similar richness values.

ter, so in the $(R_0, \alpha)$ plane, one typically expects a sharp constraint on the mean cluster radius, and a considerably weaker constraint on the orthogonal direction, corresponding to the scaling of the radius with richness around the statistical pivot point. Thus, we expect the observed degeneracy between $R_0$ and $\alpha$ to pick out parameter combinations that hold the median cluster radius of the sample fixed.

Figure 2 clearly illustrates that this is the case. In the figure, the diagonal dotted line corresponds to a contour of fixed median cluster radius $\tilde{R}(R_0, \alpha) = 900 \, h^{-1}$ kpc, where the function $\tilde{R}(R_0, \alpha)$ is defined as the median cluster radius of the 2000 richest clusters. The fact that this contour falls almost exactly along the observed degeneracy between $R_0$ and $\alpha$ strongly supports our interpretation.

Our argument suggests a way to break the degeneracy between $R_0$ and $\alpha$. If we can measure the scatter in $L_X$ at fixed richness at two very different richness scales, then the mean radius picked out by each of the samples will be substantially different. This, in turn, rotates the degeneracy lines relative to

each other, so that the intersection defined by the two samples would cleanly pick out a single value for $R_0$ and $\alpha$.

We have repeated our analysis on the top 500 and 1000 clusters, but these thresholds are much too close to our reported 2000 clusters to be able to successfully break the observed degeneracy. Ideally, we would repeat our study using the 10000 or 20000 richest clusters, thereby guaranteeing a degeneracy region that is significantly rotated relative to that of Figure 2. Unfortunately, performing our scatter analysis on the top 10000 clusters is not presently possible since the vast majority of this larger cluster sample does not emit sufficiently in X-rays to allow for individual luminosity estimates of the clusters. Furthermore, when choosing more than the top $\sim 3000$ clusters we begin to run into threshold effects due to the initial selection of maxBCG clusters with $N_{200} \geq 10$. One might hope instead to repeat our analysis using not the top 10000 clusters, but rather the top 100 clusters, that is, by limiting ourselves to the very richest systems. Unfortunately, this suffers from a different problem: when looking at the top 100 clusters only, the range of richnesses being sampled is much too narrow to allow a simultaneous estimate of the amplitude, slope, and scatter of the $L_X$-richness relation, so performing our analysis using the top 100 clusters only is also not feasible. Thus, at the time being, we must simply accept the existence of a large degeneracy between $R_0$ and $\alpha$.

### 5.2. Selecting an Optimal $\alpha$

Due to the large degeneracy between $R_0$ and $\alpha$, it is difficult to select any single point in $R_0 - \alpha$ space as optimal. We note, however, that the degeneracy region goes through $\alpha = 1/3$, which is loosely theoretically motivated based on the naive expectation $R^3 \propto M \propto \lambda$. Since our goal is to define a unique richness measure, we have opted for setting $\alpha = 1/3$. Given that the degeneracy region goes through $\alpha = 1/3$, our choice does not adversely affect the properties of our richness estimator. That is, the scatter for $\alpha = 1/3$ is indistinguishable from that of the best possible value for $\alpha$ to within observational uncertainties.

Using a principal component analysis on the best-fit minima that describe the contours in Figure 2, we have calculated the degeneracy axis for each of the full and clean cluster samples. For the full cluster sample we obtain

$$\ln(R_0 / 1 \, h^{-1} \, \text{Mpc}) - 1.342(\alpha - 0.33) = 0.25 \pm 0.04, \quad (16)$$

while for the clean cluster sample we find

$$\ln(R_0 / 1 \, h^{-1} \, \text{Mpc}) - 1.277(\alpha - 0.33) = 0.24 \pm 0.03 \quad (17)$$

We have confirmed that the residuals are Gaussian along most of the degeneracy axis. We quote the degeneracy line in terms of $\ln R_0$ and $\alpha$ rather than $R_0$ and $\alpha$ themselves simply because the former results in more accurate extrapolations for $\alpha$ values that are very different form $\alpha = 1/3$.

We are encouraged by the fact that the clean and full samples give fully consistent results, thus showing that the known cool core clusters and obvious foreground contamination are not significantly biasing the best combination of $R_0$ and $\alpha$. Our final choice for $R_0$ and $\alpha$ is therefore $R_0 = 1.27 \, h^{-1}$ Mpc and $\alpha = 1/3$.

### 5.3. Improvement in the Scatter

Now that we have a fully specified $R_0 = 1.27 \, h^{-1}$ Mpc and $\alpha = 1/3$, we have measured the matched filter richness of every cluster in the Koester et al. (2007b) sample. Figure 3

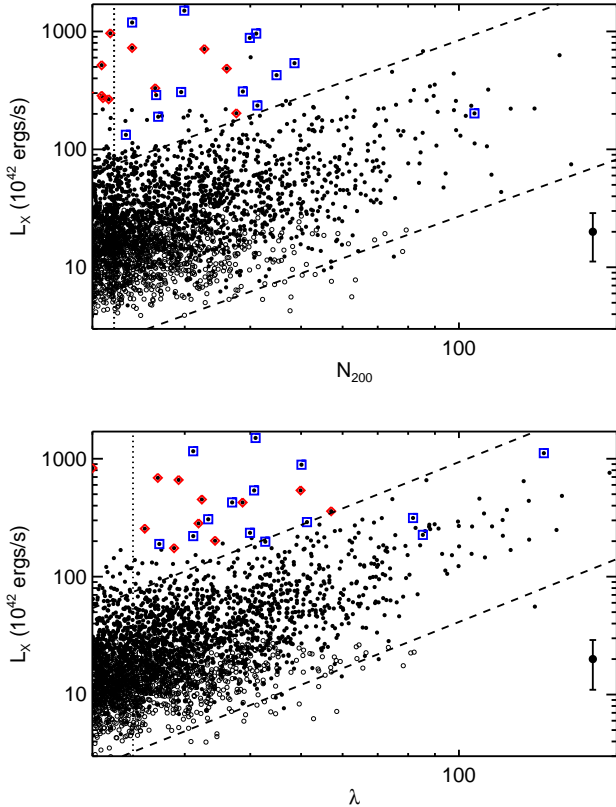TABLE 1. SCATTER IN $L_X$ AT FIXED RICHNESS, TOP 2000 CLUSTERS

| Richness | Full Sample | Clean Sample |
|---|---|---|
| $N_{200}$ | $0.95 \pm 0.03$ | $0.86 \pm 0.02$ |
| $N_{200} L_{BCG}^{0.79}$ | $0.84 \pm 0.02$ | $0.78 \pm 0.02$ |
| $\lambda$ | $0.79 \pm 0.02$ | $0.70 \pm 0.02$ |
| $\lambda$ | $0.78 \pm 0.02$ | $0.69 \pm 0.02$ |

Except for the last row, $L_X$ was measured within a fixed $1\,h^{-1}$ Mpc aperture. The scatter in $L_X$ quoted in the last row is different only in that it measured $L_X$ within the assigned optical cluster radius $R_c(\lambda)$. The combination $N_{200} L_{BCG}^{0.79}$ was suggested by Reyes et al. (2008) as an improvement over $N_{200}$. The error bars define 68% confidence intervals.

FIG. 3.— *Top panel:* $L_X$ vs. $N_{200}$ for the 3000 richest clusters. Following Rykoff et al. (2008b), the solid points represent $> 1\sigma$ detections, and the empty circles represent $1\sigma$ upper limits. The vertical dotted line represents the cutoff for the top 2000 clusters used in the analysis. The dashed lines represent the $\pm 2\sigma_{\ln L | N_{200}}$ scatter constraints. The fictitious data point in the lower-right corner shows the typical $L_X$ error. The red diamonds represent clusters that are excluded from the clean sample because they are obviously contaminated by foreground X-ray emission. The blue squares represent clusters that are excluded from the clean sample because they are known cool core clusters. *Bottom panel:* $L_X$ vs. $\lambda$ for $R_0 = 1.27$, $\alpha = 1/3$ for the 3000 richest clusters; the symbols are the same as for the top panel. Our optimized matched filter richness estimate $\lambda$ is significantly more tightly correlated with $L_X$ than $N_{200}$.

shows $L_X$ vs. $N_{200}$ (top panel) and $L_X$ vs. $\lambda$ (bottom panel) for the top 3000 richest clusters. Following Rykoff et al. (2008b), the solid points represent detections at the $> 1\sigma$ level, and the empty points represent $1\sigma$ upper limits. The vertical dotted line represents the cutoff for the top 2000 richest clusters used in this analysis. Though not obviously visible in this plot, the scatter in $\lambda$ is significantly decreased. We note that there are still some significant outliers in the $L_X - \lambda$ relation, especially at high $L_X$. The red diamonds and blue squares represent clusters that are removed from the clean cluster sample. The red diamonds are clusters whose measured X-ray flux is known to be contaminated by foreground emission from stars, nearby galaxy clusters, or AGN. The blue squares represent the known cool core clusters. These are, for the most part, significantly brighter than typical maxBCG clusters at similar richness, which is consistent with the hypothesis that the X-ray luminosity of these clusters is boosted by emission from the core.

Table 1 summarizes how the scatter of the 2000 richest clusters varies as we change our richness measure. Here, we con-

sider three richness measures only: $N_{200}$, which is the original richness estimate for maxBCG clusters presented in Koester et al. (2007a); $N_{200} L_{BCG}^{0.79}$, which was suggested by Reyes et al. (2008) as an improvement over $N_{200}$ by making use of $L_{BCG}$, the luminosity of the cluster BCG; and our optimized matched filter richness estimator $\lambda$. We see that for both the full and clean sample, our optimized matched filter estimator significantly outperforms both $N_{200}$ and $N_{200} L_{BCG}^{0.79}$. To quantify the significance of the improvement, we must take into account the fact that the errors are correlated. Following § 4, we have performed bootstrap resampling on the full catalog and clean catalog, calculating the scatter in the top 2000 clusters for both $\lambda$ and $N_{200}$. For each bootstrap resampling we calculate $r = \sigma_{\ln L_X | \lambda} / \sigma_{\ln L_X | N_{200}}$. The deviation from $r = 1.0$ can be used to quantify the significance of the improvement. The improvement in the scatter relative to $N_{200}$ is significant at $9\sigma$ for the full cluster sample, and at $11\sigma$ for the clean sample.

## 6. REDSHIFT DEPENDENCE

Rykoff et al. (2008b) showed that there is strong redshift evolution in the $\langle L_X | N_{200} \rangle$ relation of maxBCG clusters. Similar redshift dependence is observed in the velocity dispersion-optical richness relation measured in Becker et al. (2007a). This is best understood as a variation of $N_{200}$ at fixed mass, with an observed fractional decrease in $N_{200}$ of $30\% - 40\%$ over the redshift range of the maxBCG catalog. In our previous work, the origin of this redshift dependence was unclear. Here, we demonstrate how the matched-filter richness removes this redshift dependence, and show the pitfalls of a simple richness estimator such as $N_{200}$.

Figure 4 shows the $\langle L_X | N_{200} \rangle$ relation for maxBCG clusters split into three different redshift bins (solid symbols). Also shown is the mean relation $\langle L_X | \lambda \rangle$ for the same three redshift bins (empty symbols). It is obvious from the figure that the redshift evolution in the $L_X$−richness relation is significantly weaker for $\lambda$ than it is for $N_{200}$. We have fit the data with a power-law evolution in redshift, following Rykoff et al. (2008b, §5.3):

$$\langle L_X | N \rangle = A \left( \frac{N}{40} \right)^{\alpha} \left( \frac{1+z}{1+\tilde{z}} \right)^{\gamma} \qquad (18)$$

where $\tilde{z}$ is the median redshift of the cluster sample and $N$ is the richness measure of interest. We find that $\gamma = 6.0 \pm 0.8$ for $N_{200}$ while $\gamma = 0.7 \pm 0.8$ for $\lambda$, consistent with no evolution.

Note, however, that even if the relation between $\lambda$ and cluster mass is redshift independent, we expect to see evolution in the $L_X - \lambda$ relation due to evolution in the $L_X - M$ relation. The expectation for self-similar evolution in $L_X$ at fixed mass is that $L_X \propto \rho_c(z)^{7/6}$ for bolometric luminosities, but closer to
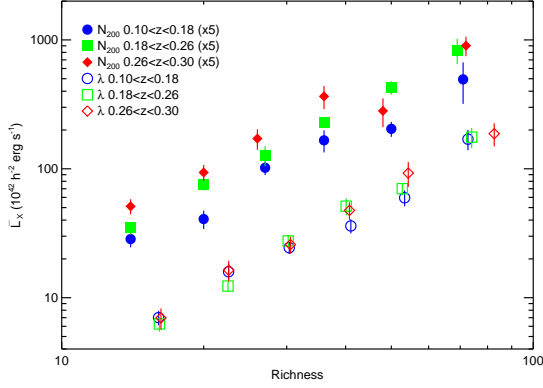
FIG. 4.— $\langle L_X \rangle$ vs. richness in three different richness bins. The empty points denote the matched filter richness $\lambda$, and the solid points denote the original maxBCG richness $N_{200}$. The three richness bins are: $0.10 < z < 0.18$ (blue circles); $0.18 < z < 0.26$ (green squares); $0.26 < z < 0.30$ (red diamonds). The normalization of $\langle L_X \rangle - N_{200}$ has been multiplied by 5 for clarity. It is readily apparent that $N_{200}$ has a strong redshift dependence (Rykoff et al. 2008b; Becker et al. 2007a), while $\lambda$ does not.

$\bar{\rho}_c^{1.0}$ for soft-band X-ray luminosities (Kaiser 1986). Here, $\rho_c$ is the critical density of the universe at redshift $z$. In a $\Lambda$CDM universe with $\Omega_m = 0.25$, the expected soft X-ray band evolution is thus $\gamma \approx 1.05$, so our results are also consistent with self-similar evolution.

The striking difference in the evolution in the $L_X$−richness relation between $\lambda$ and $N_{200}$ is due to the differences in how $N_{200}$ and $\lambda$ employ galaxy colors when estimating cluster richness. For $N_{200}$, a galaxy contributes to the richness if and only if its color differs from the BCG color by no more than twice the intrinsic width of the ridgeline color width plus the galaxy's photometric error, added in quadrature. That is, $N_{200}$ weighs galaxies according to the probability distribution $p_{top-hat}(c)$ given by:

$$p_{top-hat}(c) = \begin{cases} 1 & \text{if } |c - c_{BCG}| \le \sqrt{(2\sigma_{int})^2 + \sigma_{obs}^2} \\ 0 & \text{otherwise} \end{cases} \quad (19)$$

where $\sigma_{int} = 0.05$ is the intrinsic width of the ridgeline. This is a top-hat distribution in observed color, but the width of the top-hat depends on the photometric error of the galaxy under consideration. Also, note that the center of the color box is not the model $\langle c|z \rangle$ quoted earlier, but rather the color of the BCG, which, as we show below, is a very significant difference.

To illustrate how these differences in the color filter results in differences in the evolution and scatter of $\lambda$ and $N_{200}$, we have defined three additional richness measures with key properties bridging those of $\lambda$ and $N_{200}$. Including $\lambda$ and $N_{200}$, the five richness measures considered here are

1. $\lambda$: the matched filter richness with a variable aperture, as described above, with a gaussian color filter centered on $\langle c|z \rangle$.

2. $\lambda_{BCG}$: the matched filter richness using the same aperture as with $\lambda$, but with the Gaussian model centered on $c_{BCG}$.

3. $N_{top-hat,model}$, a top-hat richness using the $p_{top-hat}$ formulation above, centered around $\langle c|z \rangle$ as in Eqn. 11, measured on a fixed $1\,h^{-1}$ Mpc scale.

TABLE 2. SCATTER ($\sigma_{\ln L_X|N}$) AND REDSHIFT EVOLUTION ($\gamma$)

| Richness | $\sigma_{\ln L_X|N}$[a] | $\gamma$ |
|---|---|---|
| $\lambda$ | $0.78 \pm 0.02$ | $0.7 \pm 0.8$ |
| $\lambda_{BCG}$ | $0.82 \pm 0.02$ | $1.1 \pm 0.8$ |
| $N_{top-hat,model}$ | $0.80 \pm 0.02$ | $0.5 \pm 0.8$ |
| $N_{top-hat,BCG}$ | $0.99 \pm 0.02$ | $4.2 \pm 0.7$ |
| $N_{200}$ | $0.95 \pm 0.02$ | $6.0 \pm 0.8$ |

[a]For the top 2000 clusters

4. $N_{top-hat,BCG}$, a top-hat richness using the $p_{top-hat}$ formulation above, centered around $c_{BCG}$, measured on a fixed $1\,h^{-1}$ Mpc scale. This is similar to the maxBCG $N_{gals}$ richness, without the additional cut on the $r-i$ color of the member galaxies.

5. $N_{200}$, the original maxBCG richness estimator, measured in a scaled radius $r_{200}^{gals}$, with the color filter centered on $c_{BCG}$.

Table 2 shows the scatter (in the top 2000 clusters) and evolution parameters for these various richness estimators. There are two key observations that we can make here. First, when using the top-hat richness, centering around the model color is significantly better than centering on the BCG color, in terms of decreasing both the scatter and evolution of the richness measure. Second, the smooth Gaussian filter centered on the BCG color works almost as well as the Gaussian filter centered on the model color. This is a significant result, because it implies that not only are the resulting richnesses more robust to moderate changes in the color filter parameters, but also the richness measure itself is also robust to photometric redshift errors. The reason for this robustness is simple: when using a color top-hat selection, using the correct color model is of paramount of importance since miscentering of the top-hat will lead to underestimates of the richness. In the matched filter framework, what is important is the relative galaxy density of the cluster and field components, which can remain high even if the centering of the ridgeline color is slightly displaced. Thus, matched-filter richness estimates are much more robust to small changes in the parameters of the color filter than estimates based on simple color cuts.

As an illustration of this effect, Figure 5 shows the color distribution of all galaxies brighter than $0.4L_*$ within $1\,h^{-1}$ Mpc (solid black line) of the galaxy cluster SDSS J082026.8+073650.1 at a redshift $z_{spec} = 0.22$. This cluster was selected because of the large discrepancy between $N_{200}$ and $\lambda$. The color of the cluster BCG (solid red line) is significantly redder than the red sequence. The dotted vertical lines show the $\pm 2\sigma_{int}$ color cut, which does not include the peak of the red sequence. As a result, $N_{200}$ is significantly underestimated in this system. The blue curve shows the same galaxy distribution, but weighing each galaxy by its membership probability as estimated using the matched filter approach. As we can see, the matched filter effectively selects galaxies in the red sequence.

We have demonstrated that the redshift evolution observed in the $L_X - N_{200}$ relation is primarily caused by using a top-hat filter centered on the color of the BCG. Why such a choice of color filter results in the strong evolution we observe for $N_{200}$ is a complicated question, with at least two physical mechanisms contributing to the problem at comparable levels. First,
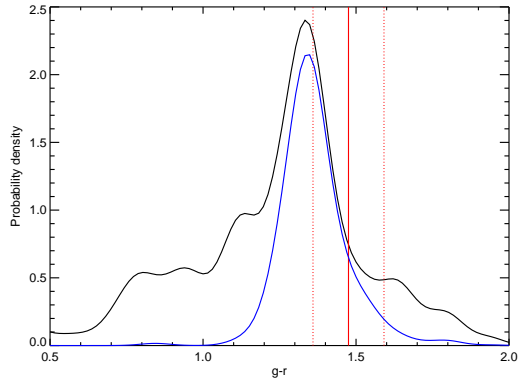
FIG. 5.— Color distribution of all the galaxies brighter than $0.4 L_*$ within $1 h^{-1}$ Mpc (solid black line) of the galaxy cluster SDSS J082026.8+073650.1 at a redshift of $z_{spec} = 0.22$. The distribution is estimated using a Gaussian Kernel Density Estimator (KDE), with the size of the kernel selected to adequately sample the peak due to ridgeline galaxies. The cluster BCG color (solid red line) is significantly redder than the red sequence (peak of the black distribution). The dotted vertical lines show the $\pm 2\sigma_{int}$ color cut, which does not include the bulk of the red sequence, and therefore $N_{200}$ is significantly underestimated. The blue curve is the KDE estimate of the galaxy distribution, except every galaxy has been weighted by its membership probability as estimated using the matched filter approach. We can see the match filter richness estimate selects principally ridgeline galaxies.

there is the fact that even for a correctly centered top-hat filter, a ridgeline galaxy can fall outside the color cuts due to photometric errors. Since photometric errors increase with increasing redshift, a color cut such as that of $N_{200}$ will progressively lose more galaxies as one moves the cluster to higher redshift. Second, the E/S0 ridgeline is not flat, but has a slight tilt ($\sim -0.04$ mags/mag in $g-r$ vs. $i$), such that brighter galaxies tend to be redder (e.g. Visvanathan & Sandage 1977; Renzini 2006). By centering the color filter on the BCG – by definition the brightest and usually reddest cluster member – a small richness bias is introduced: clusters with brighter BCGs have a color filter centered redward of the average BCG color. Moreover, recent work by Hao et al. (in preparation) shows that with a proper account for photometric errors, the ridgeline tilt evolves with redshift, such that the ridgeline is *steeper* at $z = 0.3$ than at $z = 0.1$. Consequently, a BCG centered color cut becomes increasingly offset from the true mean ridgeline color as we increase redshift. Both of these systematics effects occur with similar magnitude, and act in concert to produce the observed evolution in $N_{200}$. We emphasize, however, that our matched filter richness estimator does *not* suffer from these systematic effects.

Finally, we can now also explain why $N_{200}$ exhibits stronger evolution than $N_{top-hat,BCG}$. Recall that the aperture used to estimate $N_{200}$ is itself based on the richness measure $N_{gals}$, which is very similar to $N_{top-hat,BCG}$. Since $N_{top-hat,BCG}$ systematically underestimates the richness for high redshift clusters due to the increasing tilt of the ridgeline, the aperture $r_{200}^{gals}$, which scales with $N_{top-hat,BCG}$, is also underestimated. This compounds the effect of incorrect centering of the color box and results in stronger redshift evolution.

## 7. SUMMARY AND CONCLUSIONS

We have introduced a new matched filter richness estimator $\lambda$ whose correlation with mass is significantly tighter than that of $N_{200}$, the original maxBCG richness estimator. Relative to other matched filter estimates, our estimator has two significant differences:

1. The richness is measured on a scale that is optimized in the sense that it minimizes the scatter in $L_X$ at fixed richness.

2. In addition to a radial and magnitude filters, we include a color filter. This is of crucial importance for differentiating between member and non-member (projected) galaxies.

The first these points is important since we have demonstrated that a poor choice of aperture increases the scatter in mass at fixed richness, while the latter minimizes the impact of projection effects in richness estimates. Of the two, however, the improved treatment of galaxy color is the principal reason for the marked reduction of the scatter in the $L_X$−richness relation.

Our procedure for aperture optimization can be easily generalized to any mass tracer for which one can construct a calibrating data set. In our particular case, we minimize the scatter in the $L_X - \lambda$ relation by measuring both $L_X$ and $\lambda$ within an aperture $R_c(\lambda) = R_0(\lambda/100)^{\alpha}$, and varying the model parameters $R_0$ and $\lambda$. Given the small richness range probed by our sample, we have not been able to isolate unique values for $R_0$ and $\alpha$, finding instead a degeneracy region corresponding to a fixed mean cluster radius for the clusters in the sample. Based on *a priori* assumptions about the radius–richness scaling, we have fixed $\alpha = 1/3$, which yields a normalization of $R_0 = 1.27 \pm 0.03$. We note, however, that the degeneracy region intersects $\alpha = 0$ at $R_0 \approx 850 h^{-1}$ kpc. Although we expect that this fixed scaling will not be ideal at the rich group/poor cluster scale, it does work as a "first guess" richness and may be applicable to future cluster finding techniques. At this point, it is unclear whether the cluster radii selected by our technique reflects a true physical property of the maxBCG clusters, or whether it is driven primarily by a compromise between the the increase signal one expects at larger aperture, and the smaller noise one expects for smaller apertures. Regardless of the source, it is likely that similar aperture dependences exist for other mass tracers.

We have also found our new richness estimator has scaling relations whose redshift evolution is much more mild than those exhibited by $N_{200}$. This difference arises due to two effects: first, $N_{200}$ uses a top-hat filter to select cluster galaxies, where as our matched filter estimator $\lambda$ uses gaussian color filters. Second, $N_{200}$ centered its color filter at the color of the BCG, whereas $\lambda$ centered its color using an observationally calibrated color–redshift relation. The fact that the color of the BCG does not always agree with the observationally calibrated redshift-color relation leads to a systematic difference between the two richness measures. Moreover, we also found that the sharp edges of the top-hat filter result in a richness estimator that is very sensitive to the details of the color model, whereas our gaussian filter is much more robust to moderate changes in the model parameters.

Restricting ourselves to the clean cluster sample, which excludes cooling flow clusters and clusters with obvious foreground contamination in their X-ray luminosities, we have found that the scatter in the $L_X$−richness relation of the 2000 richest clusters is is $\sigma_{\ln L_X | \lambda} = 0.69$ for $\lambda$, compared to $\sigma_{\ln L_X | N_{200}} = 0.86$ for $N_{200}$. Assuming a slope of $\approx 1.6$ for the $L_X - M$ relation (Stanek et al. 2006; Rykoff et al. 2008a; Vikhlinin et al. 2008a), these amount to a logarithmic scatter in the mass–richness relation of $\approx 0.43$ and $0.54$ respectively.

While this is a very significant improvement, we expect that further tightening of the scatter in mass at fixed richness must be possible. For instance, assuming the intrinsic scatter in the richness-mass relation is Poisson, the logarithmic scatter possible for clusters with 20 galaxies or so should be roughly $\approx 0.2$.

Fortunately, there are still many options left for us to explore in our quest to define optical mass proxies that can be competitive with other mass tracers in terms of the tightness of the correlation with mass. As we have defined it here, our richness estimates only makes use of the number of galaxies in the cluster. One could, for instance, weigh our cluster richness by other optical mass tracers such as the luminosity of the brightest cluster galaxy (Reyes et al. 2008), the abundance of baryons contained in the intracluster light (e.g. Gonzalez et al. 2007), or other aspects of the cluster galaxy morphology (e.g. Bautz-Morgan Type, Bautz & Morgan 1970). In addition, one could weigh each galaxy's contribution to the richness by physical observables such as galaxy luminosity. Such a luminosity weighted richness estimate would be a measure of the optical luminosity of the cluster as a whole, and might be better correlated with mass than richness itself (see also Lin et al. 2003; Miller et al. 2005; Popesso et al. 2005). It is also likely that further improvements in richness estimates can arise with more accurate filters, a possibility we intend to explore in future work. Finally, we know that even with today's filters, part of the scatter we observe must be due to systematics effects such as failures of the cluster finding algorithm in identifying the correct center of a cluster, a problem which we have not addressed in this work. For the time being, the fact that naive theoretical expectations result in a scatter much lower than previously observed, and the fact that on our first attempt at defining a better richness estimator resulted in a highly significant ($\approx 11\sigma$) improvement over $N_{200}$, suggest that the future is rife with opportunities for this kind of work.

## REFERENCES

Abell, G. O. 1958, ApJS, 3, 211
Abell, G. O., Corwin, Jr., H. G., & Olowin, R. P. 1989, ApJS, 70, 1
Adelman-McCarthy, J. K. et al. 2008, ApJS, 175, 297
—. 2006, ApJS, 162, 38
Bahcall, N. A. 1981, ApJ, 247, 787
Bartelmann, M. 1996, A&A, 313, 697
Bauer, F. E., Fabian, A. C., Sanders, J. S., Allen, S. W., & Johnstone, R. M. 2005, MNRAS, 359, 1481
Bautz, L. P., & Morgan, W. W. 1970, ApJ, 162, L149+
Becker, M. R. et al. 2007b, ApJ, 669, 905
—. 2007a, ApJ, 669, 905
Böhringer, H., Burwitz, V., Zhang, Y.-Y., Schuecker, P., & Nowak, N. 2005, ApJ, 633, 148
Böhringer, H. et al. 2004, A&A, 425, 367
Bond, J. R., Cole, S., Efstathiou, G., & Kaiser, N. 1991, ApJ, 379, 440
Bower, R. G., Lucey, J. R., & Ellis, R. S. 1992, MNRAS, 254, 601
Bramel, D. A., Nichol, R. C., & Pope, A. C. 2000, ApJ, 533, 601
Chen, Y., Reiprich, T. H., Böhringer, H., Ikebe, Y., & Zhang, Y.-Y. 2007, A&A, 466, 805
Cuesta, A. J., Prada, F., Klypin, A., & Moles, M. 2008, MNRAS, 846
Dai, X., Kochanek, C. S., & Morgan, N. D. 2007, ApJ, 658, 917
Dong, F., Pierpaoli, E., Gunn, J. E., & Wechsler, R. H. 2008, ApJ, 676, 868
Dressler, A. 1984, ARA&A, 22, 185
Eisenstein, D. J. et al. 2001, AJ, 122, 2267
Fukugita, M., Ichikawa, T., Gunn, J. E., Doi, M., Shimasaku, K., & Schneider, D. P. 1996, AJ, 111, 1748
Gladders, M. D., & Yee, H. K. C. 2000, AJ, 120, 2148
—. 2005, ApJS, 157, 1
Gladders, M. D., Yee, H. K. C., Majumdar, S., Barrientos, L. F., Hoekstra, H., Hall, P. B., & Infante, L. 2007, ApJ, 655, 128
Gonzalez, A. H., Zaritsky, D., & Zabludoff, A. I. 2007, ApJ, 666, 147
Goto, T. et al. 2002, AJ, 123, 1807
Gunn, J. E. et al. 2006, AJ, 131, 2332
Haiman, Z., Mohr, J. J., & Holder, G. P. 2001, ApJ, 553, 545

Hansen, S. M., McKay, T. A., Wechsler, R. H., Annis, J., Sheldon, E. S., & Kimball, A. 2005, ApJ, 633, 122
Hansen, S. M., Sheldon, E. S., Wechsler, R. H., & Koester, B. P. 2007, ArXiv e-prints, 710, astro-ph/0710.3780
Hockney, R. W., & Eastwood, J. W. 1981, Computer Simulation Using Particles (Computer Simulation Using Particles, New York: McGraw-Hill, 1981)
Hogg, D. W., Finkbeiner, D. P., Schlegel, D. J., & Gunn, J. E. 2001, AJ, 122, 2129
Holder, G., Haiman, Z., & Mohr, J. J. 2001, ApJ, 560, L111
Hu, W., & Cohn, J. D. 2006, Phys. Rev. D, 73, 067301
Jenkins, A., Frenk, C. S., White, S. D. M., Colberg, J. M., Cole, S., Evrard, A. E., Couchman, H. M. P., & Yoshida, N. 2001, MNRAS, 321, 372
Johnston, D. E. et al. 2007, ArXiv e-prints, 709, astro-ph/0709.1159
Kaiser, N. 1986, MNRAS, 222, 323
Kelly, B. C. 2007, ApJ, 665, 1489
Kochanek, C. S., White, M., Huchra, J., Macri, L., Jarrett, T. H., Schneider, S. E., & Mader, J. 2003, ApJ, 585, 161
Koester, B. P. et al. 2007a, ApJ, 660, 239
—. 2007b, ApJ, 660, 221
Kormendy, J., & Djorgovski, S. 1989, ARA&A, 27, 235
Kravtsov, A. V., Vikhlinin, A., & Nagai, D. 2006, ApJ, 650, 128
Lima, M., & Hu, W. 2004, Phys. Rev. D, 70, 043504
—. 2005, Phys. Rev. D, 72, 043006
Lin, Y.-T., & Mohr, J. J. 2004, ApJ, 617, 879
Lin, Y.-T., Mohr, J. J., & Stanford, S. A. 2003, ApJ, 591, 749
Lupton, R., Gunn, J. E., Ivezić, Z., Knapp, G. R., & Kent, S. 2001, in Astronomical Society of the Pacific Conference Series, Vol. 238, Astronomical Data Analysis Software and Systems X, ed. F. R. Harnden, Jr., F. A. Primini, & H. E. Payne, 269–+
Majumdar, S., & Mohr, J. J. 2004, ApJ, 613, 41
Martínez, H. J., & Muriel, H. 2006, MNRAS, 370, 1003
Martínez, H. J., Zandivarez, A., Domínguez, M., Merchán, M. E., & Lambas, D. G. 2002, MNRAS, 333, L31
Maughan, B. J. 2007, ApJ, 668, 772

Miller, C. J. et al. 2005, AJ, 130, 968
Muzzin, A., Yee, H. K. C., Hall, P. B., & Lin, H. 2007, ApJ, 663, 150
Navarro, J. F., Frenk, C. S., & White, S. D. M. 1995, MNRAS, 275, 56
—. 1997, ApJ, 490, 493 (NFW)
O'Hara, T. B., Mohr, J. J., Bialek, J. J., & Evrard, A. E. 2006, ApJ, 639, 64
Peres, C. B., Fabian, A. C., Edge, A. C., Allen, S. W., Johnstone, R. M., & White, D. A. 1998, MNRAS, 298, 416
Pier, J. R., Munn, J. A., Hindsley, R. B., Hennessy, G. S., Kent, S. M., Lupton, R. H., & Ivezić, Ž. 2003, AJ, 125, 1559
Popesso, P., Biviano, A., Böhringer, H., & Romaniello, M. 2007, A&A, 464, 451
Popesso, P., Biviano, A., Böhringer, H., Romaniello, M., & Voges, W. 2005, A&A, 433, 431
Postman, M., Lubin, L. M., Gunn, J. E., Oke, J. B., Hoessel, J. G., Schneider, D. P., & Christensen, J. A. 1996, AJ, 111, 615
Press, W. H., & Schechter, P. 1974, ApJ, 187, 425
Reiprich, T. H., & Böhringer, H. 2002, ApJ, 567, 716
Renzini, A. 2006, ARA&A, 44, 141
Reyes, R., Mandelbaum, R., Hirata, C. M., Bahcall, N., & Seljak, U. 2008, ArXiv e-prints, 802, astro-ph/0802.2365
Rozo, E., Dodelson, S., & Frieman, J. A. 2004, Phys. Rev. D, 70, 083008
Rozo, E. et al. 2007, ArXiv Astrophysics e-prints, astro-ph/0703571
Rozo, E., et al. 2008, ArXiv e-prints, 809, astro-ph/0809.2794
Rykoff, E. S. et al. 2008a, MNRAS, L58+
—. 2008b, ApJ, 675, 1106
Sheldon, E. S. et al. 2007a, ArXiv e-prints, 709
—. 2007b, ArXiv e-prints, 709, astro-ph/0709.1153

Sheth, R. K., & Tormen, G. 2002, MNRAS, 329, 61
Smith, J. A. et al. 2002, AJ, 123, 2121
Stanek, R., Evrard, A. E., Böhringer, H., Schuecker, P., & Nord, B. 2006, ApJ, 648, 956
Strauss, M. A. et al. 2002, AJ, 124, 1810
Tinker, J. L., Kravtsov, A. V., Klypin, A., Abazajian, K., Warren, M. S., Yepes, G., Gottlober, S., & Holz, D. E. 2008, ArXiv e-prints, 803, astro-ph/0803.2706
Tucker, D. L. et al. 2006, Astronomische Nachrichten, 327, 821
Vikhlinin, A. et al. 2008a, ArXiv e-prints, 805, astro-ph/0805.2207
—. 2008b, ArXiv e-prints, 805, astro-ph/0805.2207
Visvanathan, N., & Sandage, A. 1977, ApJ, 216, 214
Voges, W. et al. 1999, A&A, 349, 389
Warren, M. S., Abazajian, K., Holz, D. E., & Teodoro, L. 2006, ApJ, 646, 881
Weinmann, S. M., van den Bosch, F. C., Yang, X., & Mo, H. J. 2006, MNRAS, 366, 2
White, S. D. M., Efstathiou, G., & Frenk, C. S. 1993, MNRAS, 262, 1023
Wu, H.-Y., Rozo, E., & Wechsler, R. H. 2008, ArXiv e-prints, 803, astro-ph/0803.1491
Yee, H. K. C., & Ellingson, E. 2003, ApJ, 585, 215
Yee, H. K. C., & López-Cruz, O. 1999, AJ, 117, 1985
York, D. G., Adelman, J., Anderson, J. E., Anderson, S. F., Annis, J., & the SDSS collaboration. 2000a, AJ, 120, 1579
York, D. G. et al. 2000b, AJ, 120, 1579

## APPENDIX

## A MAXIMUM LIKELIHOOD DERIVATION OF MATCHED FILTER RICHNESS ESTIMATORS

Here, we derive equation 2 using a maximum likelihood approach, focusing first in the case where the filters $u(\mathbf{x}|\lambda)$ are richness independent. The derivation is as follows: we pixelize the observable space $\mathbf{x}$ into infinitesimal pixels of "volume" $\Delta\mathbf{x}$ such that every pixel contains at most one galaxy. The likelihood that a given galaxy realization occurs is simply

$$\mathcal{L} \propto \prod_{occupied} (\lambda u + b)\Delta\mathbf{x} \prod_{empty} (1-(\lambda u + b)\Delta\mathbf{x}) \tag{A1}$$

where the first product is over all occupied pixels, while the second product is over all empty pixels. We have neglected terms that do not depend on $\lambda$ as they will not contribute to the maximum likelihood richness estimator. Setting $\partial\ln\mathcal{L}/\partial\lambda = 0$, and taking the limit $\Delta\mathbf{x}\to 0$ we find that the maximum likelihood richness estimator $\hat{\lambda}_{ML}$ is given by the solution to

$$1 = \sum \frac{u}{\lambda u + b} \tag{A2}$$

where the sum is over all galaxies in the cluster field. This expression is identical to our naive richness estimator from equation 2.

We wish to briefly consider how richness dependent filters $u(\mathbf{x}|\lambda)$ affect the maximum likelihood richness estimator. To do this, we go back to equation A1. Taking the derivative of the log-likelihood with respect to $\lambda$ and setting it to zero we find that the generalization of equation 2 is given by

$$1 + \int d\mathbf{x}\,\lambda\frac{\partial u}{\partial\lambda} = \sum \frac{u+\lambda(\partial u/\partial\lambda)}{\lambda u + b}. \tag{A3}$$

We emphasize that the integral over $\mathbf{x}$ and the derivative $\partial/\partial\lambda$ do *not* always commute. Indeed, consider the approach taken in this paper, in which $u$ is taken to have a finite spatial extent of radius $R_c$, which is itself linked to richness via equation 3. The fact that $u$ is zero for $R > R_c(\lambda)$ implies that the integration region for $u$ is $\lambda$ dependent, and thus the integral and derivative signs do not commute.

To assess the impact of a richness dependent profile, we consider here a simple isothermal filter $u(R|\lambda) = 1/R_c$, where $R_c(\lambda)$ is given by equation 3.[19] For this filter, we have then

$$\lambda\frac{\partial u}{\partial\lambda} = \lambda\frac{\partial u}{\partial R_c}\frac{\partial R_c}{\partial\lambda} = -\alpha u \tag{A4}$$

where $\alpha$ is the slope of the radius-richness relation in equation 3. Our expression for the maximum likelihood richness estimator becomes

$$(1-\alpha) = \sum_{R < R_c(\lambda)} \frac{(1-\alpha)u}{\lambda u + b}. \tag{A5}$$

We see that the $1-\alpha$ prefactors cancel on both side of the equation, and thus our final expression for the maximum likelihood richness estimator for $\lambda$ is still given by equation 4, even though $u$ is explicitly richness dependent. This suggests that our naive estimator is in general very close to the true maximum likelihood estimator. We defer a detailed study of whether the more complicated structure of the true maximum likelihood richness estimator for more elaborate cluster profiles can lead to a significant improvement over the naive richness estimator from equation 4 to future work.

---

[19] The two dimensional density profile is, of course, $\Sigma(R) \propto 1/R$, but the radial probability density is $u(R) = 2\pi R\Sigma(R) = 1/R_c$.